Lattice Dynamic and Instability in Pentasilicene: A Light Single-Element Ferroelectric Material With High Curie Temperature

Yaguang Guo,[1] Cunzhi Zhang,[1] Jian Zhou,[2] Qian Wang,[1,3,*] and Puru Jena[3]

[1] *Center for Applied Physics and Technology, Department of Materials Science and Engineering, HEDPS, BKL-MEMD, College of Engineering, Peking University, Beijing 100871, China*

[2] *Center for Advancing Materials Performance from the Nanoscale, State Key Laboratory for Mechanical Behavior of Materials, Xi'an Jiaotong University, Xi'an 710049, China*

[3] *Department of Physics, Virginia Commonwealth University, Richmond, Virginia 23284, USA*

(Received 20 April 2019; revised manuscript received 6 June 2019; published 26 June 2019)

The compatibility of Si semiconductor technology with current electronic devices has led to a continuing search for new Si-based materials with novel properties. The recent synthesis of penta-Si nanoribbons [Phys. Rev. Lett. 117, 276102 (2016); Nano Lett. 18, 2937 (2018); Nat. Commun. 7, 13076 (2016)] is a new addition to this family. However, pentasilicene, a two-dimensional (2D) sheet composed of only Si pentagons, was found to be unstable in pentagraphenelike configuration and could only be stabilized dynamically by surface decoration. Using first-principles calculations and a thorough analysis of its imaginary frequencies, we show that pentasilicene can indeed be made dynamically stable by tilting the Si dimers to reduce the Coulomb repulsion between them. The consequence of this tilting leads to a much more interesting discovery: the stabilized pentasilicene breaks the structural inversion symmetries, resulting in spontaneous electrical polarization and ferroelectricity with a high Curie temperature of 1190 K. This is the first report of a 2D ferroelectric system composed of a light single element, which can have potential applications in nonvolatile random access memory.

DOI: 10.1103/PhysRevApplied.11.064063

I. INTRODUCTION

Over the past few decades, silicon has been the leading material in the microelectronic industry for high-performance information storage devices. Recently, considerable effort has been made to develop nonvolatile phase change materials, such as ferroelectric or ferromagnetic RAMs, for ultrafast information storage devices down to the sub-10-nm size. In the ferroelectric phase change materials, different ferroelectric phases are separated by a high-energy barrier owing to their ionic motion. Hence, the ferroelectric phase can be well protected below the Curie temperature and the stored information can last for over 10 years. In addition, ferroelectric phase transitions are displacive and martensitic, which guarantee its faster kinetics compared to the currently used reconstructive Ge-Sb-Te alloys [1]. Two-dimensional (2D) materials have the potential to work as future nonvolatile phase change materials [2] so that electronic devices can be miniaturized into nanoscale with high information density. Thus far, Si is used as a substrate to grow ferroelectric materials (e.g., HfO_2) [3], but 2D ferroelectric phase change materials based exclusively on Si are still unknown. The reason is that once a 2D material is based on a single element (e.g., Si), positive and negative charge states are no longer separated as they are in conventional ferroelectric materials (e.g., perovskites) [4,5]. This greatly hinders the potential applications for Si electronics.

In order to separate positive and negative charge centers in a pure 2D Si material, one possible scheme is to include both sp^2 and sp^3 hybridization. Note that conventional Si compounds are composed exclusively of sp^3 hybridized Si atoms. Recently, 2D silicene (a single atomic layer Si sheet) composed of only sp^2 Si has been discovered [6]. Unfortunately, due to its zero band gap [7], 2D silicene is not suitable for information storage. Motivated by the prediction of pentagraphene [8], a 2D five-membered ring-based carbon allotrope composed of sp^2 and sp^3 hybridized carbon atoms, attempts have been made to synthesize a pentasilicene analog. However, theoretical studies showed such a structure to be dynamically unstable and it can only be stabilized by surface decoration [9,10]. Note that penta-Si nanoribbon [11–13], which exhibits exotic phenomena, such as topologically protected phases or increased spin-orbit effects [11], has already been synthesized and can be used as a building block to produce functional architectures via covalent assembly [12]. Hence, the discovery of an intrinsically stable

*qianwang2@pku.edu.cn

pentasilicenelike structure will be a welcome addition to the Si family of materials.

In this paper, we show that the desired unusual properties of Si can be realized by stabilizing Si in a quasi-2D pentagonal structure where Si dimers within a confined lattice are tilted. We label this system as *T* pentasilicene. Because the existence of soft modes of pentasilicene is due to the strong Coulomb interactions between the charged Si atoms, tilting the Si dimers can reduce Coulomb repulsion and stabilize the system. Using first-principles calculations combined with the Berry phase method and Landau-Ginzburg theory, we have not only found this tilted configuration to be *dynamically stable*, but it also leads to spontaneous electrical polarization, making *T* pentasilicene exhibit in-plane ferroelectricity with a very high Curie temperature (T_C) of 1190 K. Thus, this ferroelectric phase can be well protected under an ambient working temperature.

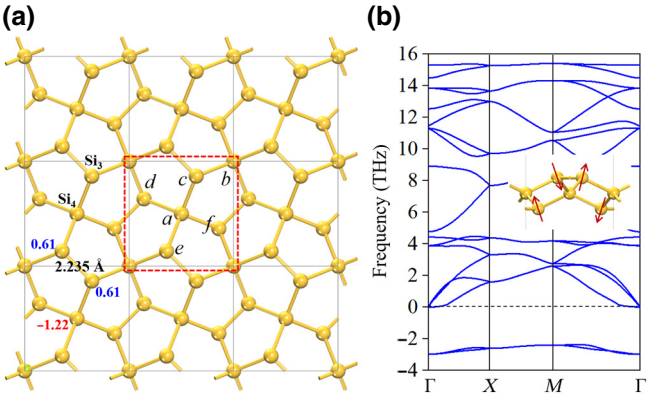

FIG. 1. (a) Top view of the pentasilicene sheet. The red-dashed square is the (*l*, *m*)th lattice point of the sheet. Indices *a*, *b*, *c*, *d*, *e*, and *f* represent different atoms in the unit cell. The blue and red numbers denote charge states. (b) Phonon spectrum of pentasilicene. The inset image shows the soft vibrational modes.

II. COMPUTATIONAL METHODS

Calculations are carried out using first-principles density-functional theory (DFT) with electronic exchange-correlation interaction treated by the Perdew-Burke-Ernzerh (PBE) functional within the generalized gradient approximation (GGA) [14]. The projector augmented wave (PAW) method [15,16] with plane-wave basis set embedded in the Vienna Ab initio Simulation Package (VASP) [17] is used to optimize the geometrical structures and study their electronic properties. The energy cutoff is set at 500 eV. The convergence criteria for energy and force are set to 0.0001 eV and 0.01 eV/Å, respectively. The Brillouin zone is represented with a $19 \times 19 \times 1$ Monkhorst-Pack special *k*-point mesh [18]. A vacuum space of 20 Å in the direction perpendicular to the sheet is used to avoid interactions between the two neighboring layers. To ensure an accurate determination of electronic properties, calculations are repeated by using the hybrid Heyd-Scuseria-Ernzerhof functional (HSE06) [19]. Phonon calculations are performed by using both the finite-displacement method [20] and density-functional perturbation theory (DFPT) method with a $5 \times 5 \times 1$ supercell, as implemented in the PHONOPY program [21]. The criteria for the energy and force convergence are 1×10^{-8} eV and 1×10^{-6} eV/Å, respectively. The intrinsic electrical polarization is calculated by using the Berry phase method [22] as implemented in VASP.

III. RESULTS AND DISCUSSION

A. Geometry and stability analysis

Figure 1(a) shows the structure of pentasilicene, which shares the same geometric feature as pentagraphene [8]. We find that the sp^3 (four-fold coordinated) and sp^2 (three-fold coordinated) Si atoms are charged, and denote them as Si_4 and Si_3, respectively. Through Bader's charge analysis, the charges on Si_3 and Si_4 are found to be $q_0 = 0.61$ and $-2q_0 = -1.22$, respectively. The phonon spectrum is plotted in Fig. 1(b). One can see that two imaginary branches appear throughout the entire Brillouin zone, which is consistent with previous results [9,10]. In order to understand the origin of the dynamic instability of this structure, we study the phonon modes by applying a classical displacement model. The total energy is estimated to contain two parts, namely, conventional elastic energy and electrostatic interactions between the charged atoms. For simplicity, we adopt a rigid ion model of atoms with Coulomb interaction and neglect the short-range Born-Mayer potential. Following the general notations in lattice dynamics, the position of atom κ in the *l*th lattice is $\mathbf{r}\binom{l}{\kappa}$ and $\mathbf{r}_{ij} = \mathbf{r}\binom{l_j\ l_i}{\kappa_j\ \kappa_i} = \mathbf{r}\binom{l_j}{\kappa_j} - \mathbf{r}\binom{l_i}{\kappa_i}$. Thus, the total energy can be written as

$$E = E_{\text{elastic}} + E_{\text{electrostatic}} = \frac{1}{2}\left(\frac{1}{2}\beta\sum_{\langle i,j\rangle} r_{ij}^2 + \sum_{i,j,j\neq i}\frac{Z_{\kappa_i}Z_{\kappa_j}}{r_{ij}}\right). \quad (1)$$

Here, i (j) is the atom index. Z and β refer, respectively, to its charge and the normalized stiffness of the spring (force constant) between the nearest neighbor i and j. The second term accounts for the Coulomb interaction. A factor of $1/2$ is used to avoid double counting. In the unit cell of pentasilicene, there are six Si atoms [labeled as *a*, *b*, *c*, *d*, *e*, and *f* in Fig. 1(a)]. Hence, the dynamic matrix of the equation of motion is an 18×18 matrix.

Because of the large size of the dynamic matrix, the dimension of such a scalar determinant needs to be reduced. By analyzing the soft vibrational modes, we find that Si_3 atoms prefer to move mainly along the

out-of-plane direction [see Fig. 1(b)]. Hence, we only consider the displacements along the z direction. In the reciprocal space, the dynamic matrix is

$$\mathbf{M} = \mathbf{D} + \mathbf{ZCZ}, \tag{2}$$

where $\mathbf{D}$ is a 6×6 dynamic matrix resulting from the springlike force without Coulomb interaction. $\mathbf{Z}$ is the charge matrix, $\mathbf{Z} = \mathrm{diag}\,[-2q_0, -2q_0, q_0, q_0, q_0, q_0,]$, and matrix $\mathbf{C}$ is independent of the charge and mass of ions

$$\mathbf{C}\begin{pmatrix} \mathbf{q} \\ \kappa\ \kappa' \end{pmatrix} = -2\exp\left\{i\mathbf{q}\cdot\mathbf{r}\begin{bmatrix} l & l' \\ \kappa & \kappa' \end{bmatrix}\right\} \times \sum_{l',l} r^{-3}\begin{pmatrix} l & l' \\ \kappa & \kappa' \end{pmatrix}. \tag{3}$$

The square root of the eigenvalues of dynamic matrix $\mathbf{M}$ is the phonon frequency. An exact analytical solution of this dynamic matrix is very challenging. To get insights into the phonon behavior, we apply the nearest-neighbor interaction approximation (i.e., only consider the leading term of the Coulomb force) and write Newton's equation of motion as follows:

$$\begin{aligned}
M\ddot{a}_{l,m} &= \beta_1[(c_{l,m} - a_{l,m}) + (d_{l,m} - a_{l,m}) + (e_{l,m} - a_{l,m}) \\
&\quad + (f_{l,m} - a_{l,m})] + C_A^{3-4}[(c_{l,m} - a_{l,m}) \\
&\quad + (d_{l,m} - a_{l,m}) + (e_{l,m} - a_{l,m}) + (f_{l,m} - a_{l,m})], \\
M\ddot{b}_{l,m} &= \beta_1[(c_{l,m} - b_{l,m}) + (d_{l+1,m} - b_{l,m}) \\
&\quad + (e_{l+1,m+1} - b_{l,m}) + (f_{l,m+1} - b_{l,m})] \\
&\quad + C_A^{3-4}[(c_{l,m} - b_{l,m}) + (d_{l+1,m} - b_{l,m}) \\
&\quad + (e_{l+1,m+1} - b_{l,m}) + (f_{l,m+1} - b_{l,m})], \\
M\ddot{c}_{l,m} &= \beta_1[(a_{l,m} - c_{l,m}) + (b_{l,m} - c_{l,m})] \\
&\quad + \beta_2(e_{l,m+1} - c_{l,m}) + C_R^{3-3}(e_{l,m+1} - c_{l,m}) \\
&\quad + C_A^{3-4}[(a_{l,m} - c_{l,m}) + (b_{l,m} - c_{l,m})], \\
M\ddot{d}_{l,m} &= \beta_1[(a_{l,m} - d_{l,m}) + (b_{l-1,m} - d_{l,m})] \\
&\quad + \beta_2[f_{l-1,m} - d_{l,m}] + C_R^{3-3}(f_{l-1,m} - d_{l,m}) \\
&\quad + C_A^{3-4}[(a_{l,m} - d_{l,m}) + (b_{l-1,m} - d_{l,m})], \\
M\ddot{e}_{l,m} &= \beta_1[(a_{l,m} - e_{l,m}) + (b_{l-1,m-1} - e_{l,m})] \\
&\quad + \beta_2(c_{l,m-1} - e_{l,m}) + C_R^{3-3}(c_{l,m-1} - e_{l,m}) \\
&\quad + C_A^{3-4}[(a_{l,m} - e_{l,m}) + (b_{l-1,m-1} - e_{l,m})], \\
M\ddot{f}_{l,m} &= \beta_1[(a_{l,m} - f_{l,m}) + (b_{l,m-1} - f_{l,m})] \\
&\quad + \beta_2(d_{l+1,m} - f_{l,m}) + C_R^{3-3}(d_{l+1,m} - f_{l,m}) \\
&\quad + C_A^{3-4}[(a_{l,m} - f_{l,m}) + (b_{l,m-1} - f_{l,m})],
\end{aligned} \tag{4}$$

where M is the mass of a Si atom, β_1 and β_2 are the spring stiffnesses of Si_3-Si_4 and Si_3-Si_3, and the C_R^{3-3} and C_A^{3-4} are, respectively, the constants of Coulomb repulsive and attractive forces, which have the following expressions:

$$C_R^{3-3} = -\frac{2|Z_i^{Si_3}||Z_j^{Si_3}|}{|\vec{r}_i^{Si_3} - \vec{r}_j^{Si_3}|^3}, \quad C_A^{3-4} = \frac{2|Z_i^{Si_3}||Z_j^{Si_4}|}{|\vec{r}_i^{Si_3} - \vec{r}_j^{Si_4}|^3}. \tag{5}$$

By solving these equations (see Text S1 in the Supplemental Material for details [23]), we find that the degenerate imaginary frequencies in the pentasilicene sheet [see Fig. 1(b)] are mainly determined by the sum of β_1, β_2, C_A^{3-4}, and C_R^{3-3}. It is confirmed that the first three terms are positive, while C_R^{3-3} is negative (details can be found in Text S2 of the Supplemental Material [23]). Thus, the Coulomb repulsions from Si_3-Si_3 contribute a negative sign to $\mathbf{M}$, which destabilizes the system.

This suggests that an effective way to stabilize pentasilicene would be to reduce the Coulomb repulsive force. Similar to Pandey's chain buckling of a Si(111) (2×1) reconstructed surface [24–26], we find that a small tilt of Si_3 dimers can lower the energy and stabilize the phonon dispersions, leading to the formation of a stable structure, T pentasilicene, as shown in Fig. 2(a). Different from the flat Si_3 dimer in pentasilicene [Fig. 1(b)], one Si_3 atom moves away from the sheet (denoted as $Si_{3,o}$, toward the sp^3 configuration) and the other Si_3 atom moves toward the sheet (denoted as $Si_{3,i}$, toward the sp^2 configuration). Note that the movement of Si_3 atoms follows the eigenvectors of the soft modes [see red arrows in Fig. 1(b)]. After geometry optimization, the bond length of $Si_{3,o}$-$Si_{3,i}$ is 2.26 Å, and they carry charges $q_{3,o} = 0.70$ and $q_{3,i} = 0.52$, respectively. The space group of T pentasilicene is reduced from $P\bar{4}2_1m$ to $P2_1$. Compared with pentasilicene [Fig. 1(a)], the numerator $\left(Z_i^{Si_3}Z_j^{Si_3}\right)$ of Eq. (5) decreases, while the denominator $\left(|\vec{r}_i^{Si_3} - \vec{r}_j^{Si_3}|^3\right)$ increases, thereby reducing the value of C_R^{3-3}. Consequently, the total energy of the system is lowered by 81 meV/cell due to the reduced

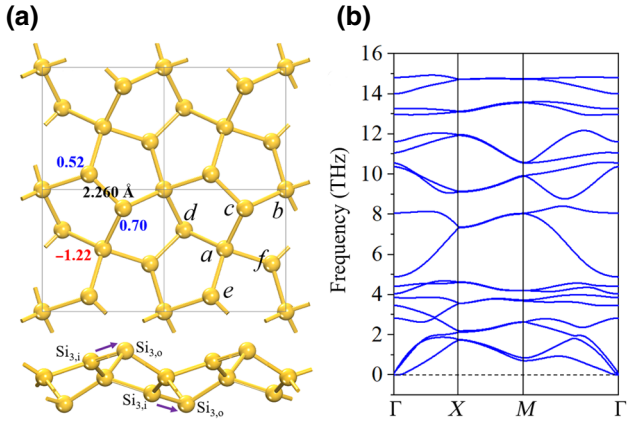

FIG. 2. (a) Atomic geometry and (b) phonon spectrum along the high symmetric k-path of T pentasilicene.

Coulomb repulsion. The enhanced stability is verified by the phonon spectrum as shown in Fig. 2(b), where no imaginary frequency exists throughout the entire Brillion zone, confirming the dynamic stability of *T* pentasilicene. Note that the *T* pentasilicene sheet should be confined within a constrained lattice during the geometry optimization, otherwise it gradually undergoes a transformation into the predicted siliconeet phase [27]. This implies that a proper confining material (e.g., a metal substrate) is needed to produce *T* pentasilicene in experiments (see Text S3 of the Supplemental Material for more details [23]).

Next, we analyze the Si_3 dimers from the electronic structure point of view. The evolution of the tilted dimer bond formation is plotted in Fig. 3(a), where the dark solid circles represent the Si_3 atoms. Each Si_3 in the dimer is in a distorted sp^2 configuration, which leaves one p_z orbital as a dangling bond. These two p_z orbitals hybridize and form a π-π^* pair. However, because of the larger atomic size of a Si atom as compared to that of a C atom [28], the π bonds are not strong enough to stabilize the pentasilicene structure. Therefore, a separation in π-π^* levels occurs to further reduce the energy. This is similar to the Jahn-Teller distortion and electrons on $Si_{3,i}$ site transfer to the $Si_{3,o}$ atom [see arrows in Fig. 2(a)], forming a tilted dimer.

In Fig. 3, we also compare the bonding configuration of *T* pentasilicene with other previously discovered pentasheets [8,9,29–32]. For pentagraphene [8] [see Fig. 3(b)], the π-π^* interaction is strong with a large strain energy. Hence, the flat three-fold coordinated carbon dimers can be maintained and the symmetric configuration is dynamically stable. This is similar to the spontaneous buckling of Pandey's sp^2 dimer chain in a Si(111) (2×1) reconstructed surface, while no buckling occurs on diamond C(111) owing to the strong strain energy [24–26]. For penta-B_2C [29] [see Fig. 3(c)], since B has one valence electron less than Si, there is no extra electron on the π orbital. Thus, no extra reduction in energy can be achieved by dimer tilting. Hence, the flat configuration remains. For penta-CN_2, SiN_2, or SiP_2 [30,31] [see Fig. 3(d)], the dimers consist of group V element atoms, which have one electron more than Si. Since π and π^* orbitals are full in these cases, energy cannot be reduced by dimer tilting. As for the hydrogenated pentasilicene [9] [see Fig. 3(e)], H and Si_3 atoms form a sigma bond, which saturates the dangling bond. In this case, all of the electrons are paired, hence reducing the energy and keeping the flat configuration of the Si dimers.

B. Electronic structure

Next, we examine the electronic properties of *T* pentasilicene. In Fig. 4(a), one can see that the band edges are mainly contributed by the Si_3 atoms, similar to those in pentagraphene. Since the dimer tilting further enlarges the energy separation between the π-π^* levels, the *T*

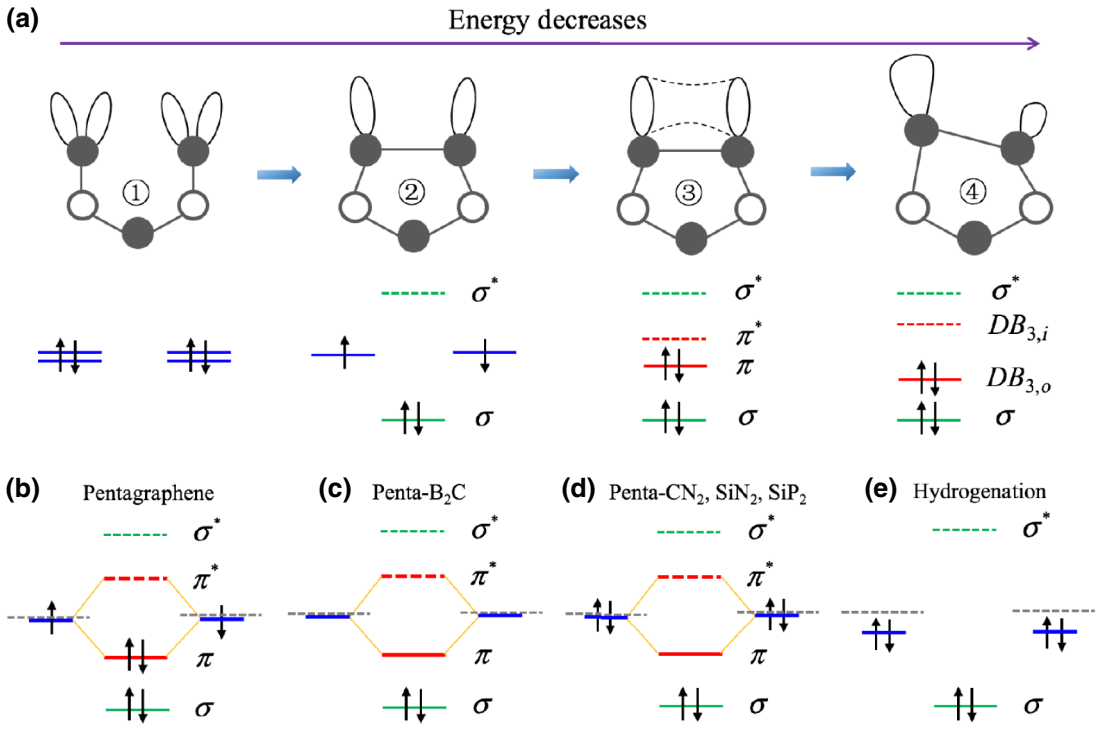

FIG. 3. (a) Understanding the dimer tilting in *T* pentasilicene. Bonding diagram of (b) pentagraphene, (c) penta-B_2C, (d) penta-CN_2, SiN_2, SiP_2, and (e) hydrogenated pentasilicene.

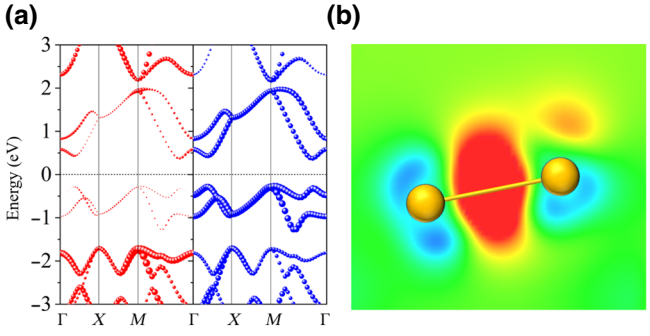

FIG. 4. (a) Band structure of *T* pentasilicene at the HSE06 level projected on Si_4 atoms (red) and Si_3 atoms (blue). (b) Charge density difference in Si_3 dimer.

pentasilicene has a larger band gap of 0.65 eV (at the HSE06 level) than that of the original configuration (0.45 eV, see Fig. S4 in the Supplemental Material [23]). The valence band maximum (VBM) and conduction band minimum (CBM) are located at different positions in the Brillouin zone, showing the signature of an indirect band gap. We note that there exists a sub-VBM close to the position of the CBM on the Γ-*M* path, thus the *T* pentasilicene can be considered as a quasidirect band-gap semiconductor. The value of this gap is close to that of the three-dimensional (3D) *h*-Si_6 allotrope [33], which may lead to a wider range of applications for *T* pentasilicene in electronics as compared with the zero-gap silicene. To better visualize the charge redistribution in the tilted Si_3 dimer, we calculate the charge density difference as shown in Fig. 4(b). The red and blue regions represent electron accumulation and depletion, respectively. It is clear that electrons on the $Si_{3,i}$ site transfer to the $Si_{3,o}$ site, which validates the bonding diagram in Fig. 3(a).

C. Ferroelectricity

The charge redistribution leads us to explore the electrical polarization of the *T* pentasilicene sheet. We find that tilting the Si_3 dimer not only lowers the total energy of the system, but also induces a polarized bond between the two nonequivalent Si_3 atoms (see Text S4 of the Supplemental Material for more details [23]). By applying the modern Berry phase theory [22,34], we calculate the electric polarization vector $\mathbf{P}_0$ of the *T* pentasilicene sheet, and find that the in-plane polarization is 18.7 pC/m (along the *x* direction), while the out-of-plane component is zero. This confirms that *T* pentasilicene is a pure Si-based 2D ferroelectric material, adding another member to the single-element ferroelectric family of As, Sb, and Bi monolayers [35]. Note that the phosphorene sheet is not electrically polarized [35]. *T* pentasilicene extends this family to the third row elements in the periodic table. Ferroelectricity in *T* pentasilicene raises another question: is an antiferroelectric (AFE) state energetically more stable? To study this, we construct a 2×2 supercell with a checkerboard pattern, where the polarization is opposite in the neighboring unit cells (see Fig. S6 in the Supplemental Material [23]). After geometry optimization, we find that the AFE configuration transforms into the ferroelectric (FE) structure, which implies that the AFE state does not exist.

One of the most important properties in a ferroelectric material is its phase transition. Because the Berry phase calculations based on DFT are performed at zero temperature, it is necessary to study the temperature range over which the ferroelectric order can survive. In general, soft modes theory is a powerful tool to study the phase transition in bulk ferroelectrics [32]. A way to estimate T_C is by simulating the behavior of phonons at a finite temperature. Unfortunately, this technique is not fully developed. Alternatively, we adopt the Landau-Ginzburg theory [36] to study the ferroelectric phase transition. Since thermodynamics governs the phase diagram, the key problem is to represent the free energy (E) as a function of the order parameter (P). To this end, we define two geometric parameters h_1 and h_2 as the bridge to connect E with P [see Fig. 5(a)]. When $h_1 = h_2 = 0$ (Phase A), the system converts back to the original pentasilicene phase, where the ferroelectric effect vanishes due to the inversion symmetry. When $h_1, h_2 > 0$ or $h_1, h_2 < 0$, the structure becomes polarized. Especially for $h_1 = h_2$, there are two stable energetically degenerate phases (B and B'), which correspond to the *T* pentasilicene structures. We note that phases B and B' can be transformed into each other by spatial inversion. Thus, if there is a polarization ($\mathbf{P}_B$) in the B phase, there must be an inverse polarization ($-\mathbf{P}_B$) in the B' phase.

Within the Landau-Ginzburg theory, we use the ϕ^4 model [37] to write E as

$$E = \sum_i \left[\frac{A}{2}(P_i^2) + \frac{B}{4}(P_i^4)\right] + \frac{C}{2}\sum_{\langle i,j\rangle}(P_i - P_j)^2, \quad (6)$$

where i and j denote the lattice points and symbol $\langle\rangle$ in the summation represents the nearest neighbor lattice site. Parameters A, B, and C are determined by fitting to the DFT data. The first two terms correspond to the energy contributed by the polarization in each unit cell, and should describe the anharmonic double-well shape of the potential profile. Note that because of spatial inversion, there only exist even powers. We neglect the higher-order terms, which are found to be less important. To obtain the values of parameters A and B, we relate E and P by mapping a series of h_1 and h_2; a direct 2D mapping is computationally costly. According to the structural symmetry of pentasilicene, we note that the variations of h_1 and h_2 are equal to each other. Thus, we only need to consider the one-dimensional (1D) parameter space, that is, $h_1 = h_2 = h$, to simplify our simulation. In practice, we calculate the total energy and polarization for each value of h. In Fig. 5(b), we plot the variation of energy (E) with respect to polarization

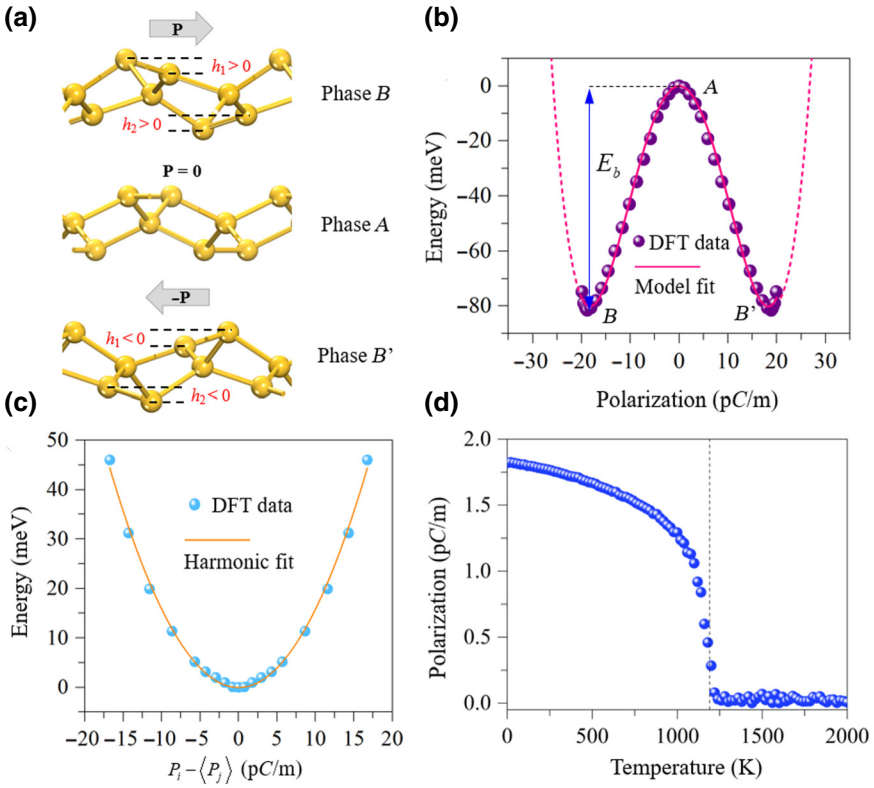

FIG. 5. (a) Schematic side views of the two degenerate ferroelectric phases (B and B') and the nonpolar phase (A). (b) Double-well potential versus polarization for T pentasilicene. E_b is the potential barrier. A, B, and B' correspond to the phases in (a). (c) The dipole-dipole interaction energy in T pentasilicene calculated by using the mean-field method. (d) Variation of polarization with temperature obtained from MC simulations for T pentasilicene.

(P). One can see that the energy profile has a double-well shape (purple balls), which is an important feature of ferroelectric materials. We observe that when h is larger than 0.57 Å, the monotonic relationship between P and h is destroyed (see Text S5 in the Supplemental Material [23]). As a result, in Fig. 5(b), we only show the DFT results with $h < 0.57$ Å, rather than the complete shape of the double-well potential. Even so, because the transition is between phases A and B (B'), the data presented in Fig. 5(b) is enough to estimate the Curie temperature. By fitting the power function, we obtain the values of parameters A (-0.962) and B (2.89×10^{-3}). The last term of Eq. (6) represents the dipole-dipole couplings between the neighboring cells, which are calculated using the supercell approach and the mean-field approximation. The DFT results with a parabola shape are plotted in Fig. 5(c), which validates the use of the second-order approximation. By fitting the points, we find parameter C to be 0.316.

Based on the effective Hamiltonian, as given in Eq. (6), we performed MC simulation to estimate T_C. To eliminate the effect of translational symmetry, a 50×50 supercell is used. We run more than 2 000 000 MC steps to reach thermal equilibrium, followed by at least another 2 000 000 MC steps to obtain thermal averages. The results of the MC simulation are plotted in Fig. 5(d). One can see that the intrinsic T_C of the T pentasilicene monolayer is about 1190 K, which is inferred from the abrupt drop of polarization around this temperature. It is important to point out that the magnitude of T_C is rather large. This is mainly caused by the higher configurational energy barrier (E_b) as shown in Fig. 5(b). In the above, we have demonstrated that the total energy difference between the original and tilted pentasilicene is 81 meV per unit cell. This value is close to $k_B T_C$ (102.55 meV), indicating that E_b plays a dominant role in determining T_C of T pentasilicene. In addition, we note that stable tilted Si dimers have been observed on a Si (001) surface at low temperatures [38]. When the temperature is elevated to 200 K, the dimer atoms start to flip in a double-well potential separated by an energy barrier of 100 meV [39]. This potential profile is exactly same as that of T pentasilicene in our study. More interestingly, analysis of the reflection high-energy electron diffraction (RHEED) rocking curve shows that there exists a phase transition of a Si (001) surface around 900 K. This corresponds to the transition of the Si dimer structure from the asymmetric to symmetric configuration [40]. This phenomenon accounts for the metallization of the Si (001) surface [41]. As mentioned before, the band gap of the T pentasilicene (0.65 eV) is larger than that of the original structure (0.45 eV). Because of these similarities (double-well potential with comparable E_b and reduction of electronic band gap), it is easy to understand that the T_C of T pentasilicene (1190 K) is close to the phase transition temperature of the Si (001) surface. Thus, we conclude that the T_C value obtained from the MC simulation is reliable.

The large T_C indicates the stability of the ferroelectric phase, making T pentasilicene a desirable material for device applications at ambient temperature. For instance,

it can potentially replace ferromagnetic RAM devices, as *T* pentasilicene combines the features of a semiconductor and ferroelectricity, while most ferromagnets are metals. In addition, compared with the insulating traditional ferroelectric materials (e.g., perovskites [4,5] and polyvinylidene difluoride [42,43]) or binary oxides (e.g., HfO_2/ZrO_2 [3]), *T* pentasilicene has a narrow band gap with dispersive band edges, as shown in Fig. 4(a). Thus, it could entail both functions of nonvolatile memory and manipulation of signals, and better transport properties can be expected to achieve high device performance. The calculated coercive electric field of *T* pentasilicene is about 0.2 V/Å. This may be a major concern for its data storage, because such a large value implies a high working voltage, which would lead to a high writing energy. However, such an electric field strength can be reduced at a finite temperature. In addition, unlike general ferroelectric materials, there is no lattice strain change during the phase transition of *T* pentasilicene. This stress-free phase transition does not have the usual stress accumulation that could induce material damage after many cycles, thus ensuring its reversibility.

The fundamental properties of *T* pentasilicene imply that it can work as a potential ferroelectric device once it is fabricated. However, the device performance does not uniquely depend on the intrinsic properties of a material. For practical applications of *T* pentasilicene, some other factors need to be considered, such as interface effects by substrate and its behavior under an external field. One also has to consider protecting it by nonreactive layers (such as BN), since sp^2 hybridized Si is chemically reactive. Hence, future insightful studies are expected to confirm our predictions on *T* pentasilicene.

IV. CONCLUSIONS

In summary, using a classical displacement model combined with DFT calculations, we show that the large Coulomb repulsion between charged Si_3 atoms accounts for the instability of pentasilicene. We predict an alternative dynamically stable *T* pentasilicene sheet composed of only Si five-membered rings, which exhibits in-plane ferroelectricity. Our study realizes spontaneous electric polarization in a light single-element system. Using Landau-Ginzburg theory, we estimate the Curie temperature of this material to be 1190 K. Such a high T_C suggests a robust ferroelectric stability of the *T* pentasilicene sheet, with potential for applications in nanoelectronic devices. Given that the *T* pentasilicene sheet is solely composed of Si atoms, it could be integrated into the well-developed Si semiconductor wafer technology. We hope that our study will stimulate more research into this material and our prediction can be experimentally validated in the near future.

ACKNOWLEDGMENTS

This work is partially supported by grants from the National Science Foundation China (Grant No. NSFC-21773004), and the National Key Research and Development Program of the Ministry of Science and Technology of China (Grants No. 2016YFE0127300 and No. 2017YFA0205003), and is supported by the High-Performance Computing Platform of Peking University, China. Y. G. acknowledges the Project funded by China Postdoctoral Science Foundation (Grant No. 2019M650289). J. Z. acknowledges the Young Talent Support Plan of Xi'an Jiaotong University. P. J. acknowledges support by the U.S DOE, Office of Basic Energy Sciences, Division of Material Sciences and Engineering under Grant No. DE-FG02-96ER45579.

[1] J. Hegedüs and S. Elliott, Microscopic origin of the fast crystallization ability of Ge-Sb-Te phase-change memory materials, Nat. Mater. **7**, 399 (2008).
[2] M. Wu and P. Jena, The rise of two-dimensional van der Waals ferroelectrics, Wiley Interdiscip. Rev.: Comput. Mol. Sci. **8**, e1365 (2018).
[3] J. Muller, T. S. Böscke, U. Schröder, S. Mueller, D. Bräuhaus, U. Böttger, L. Frey, and T. Mikolajick, Ferroelectricity in simple binary ZrO_2 and HfO_2, Nano Lett. **12**, 4318 (2012).
[4] M. Dawber, K. M. Rabe, and J. F. Scott, Physics of thin-film ferroelectric oxides, Rev. Mod. Phys. **77**, 1083 (2005).
[5] N. Sai, A. M. Kolpak, and A. M. Rappe, Ferroelectricity in ultrathin perovskite films, Phys. Rev. B **72**, 020101 (2005).
[6] P. Vogt, P. De Padova, C. Quaresima, J. Avila, E. Frantzeskakis, M. C. Asensio, A. Resta, B. Ealet, and G. Le Lay, Silicene: Compelling Experimental Evidence for Graphenelike Two-Dimensional Silicon, Phys. Rev. Lett. **108**, 155501 (2012).
[7] S. Cahangirov, M. Topsakal, E. Aktürk, H. Şahin, and S. Ciraci, Two-and One-Dimensional Honeycomb Structures of Silicon and Germanium, Phys. Rev. Lett. **102**, 236804 (2009).
[8] S. Zhang, J. Zhou, Q. Wang, X. Chen, Y. Kawazoe, and P. Jena, Penta-graphene: A new carbon allotrope, Proc. Natl. Acad. Sci. U.S.A. **112**, 2372 (2015).
[9] Y. Ding and Y. Wang, Hydrogen-induced stabilization and tunable electronic structures of penta-silicene: A computational study, J. Mater. Chem. C **3**, 11341 (2015).
[10] Y. Aierken, O. Leenaerts, and F. M. Peeters, A first-principles study of stable few-layer penta-silicene, Phys. Chem. Chem. Phys. **18**, 18486 (2016).
[11] J. I. Cerdá, J. Sławińska, G. Le Lay, A. C. Marele, J. M. Gómez-Rodríguez, and M. E. Dávila, Unveiling the pentagonal nature of perfectly aligned single-and double-strand Si nano-ribbons on Ag(110), Nat. Commun. **7**, 13076 (2016).
[12] G. Prévot, C. Hogan, T. Leoni, R. Bernard, E. Moyen, and L. Masson, Si Nanoribbons on Ag(110) Studied by Grazing-Incidence x-Ray Diffraction, Scanning Tunneling Microscopy, and Density-Functional Theory: Evidence of

a Pentamer Chain Structure, Phys. Rev. Lett. **117**, 276102 (2016).
[13] S. Sheng, R. Ma, J. B. Wu, W. Li, L. Kong, X. Cong, D. Cao, W. Hu, J. Gou, J. W. Luo, P. Cheng, P. H. Tan, Y. Jiang, L. Chen, K. Wu, The pentagonal nature of self-assembled silicon chains and magic clusters on Ag(110), Nano Lett. **18**, 2937 (2018).
[14] J. P. Perdew, K. Burke, and M. Ernzerhof, Generalized Gradient Approximation Made Simple, Phys. Rev. Lett. **77**, 3865 (1996).
[15] G. Kresse and D. Joubert, From ultrasoft pseudopotentials to the projector augmented-wave method, Phys. Rev. B **59**, 1758 (1999).
[16] P. E. Blöchl, Projector augmented-wave method, Phys. Rev. B **50**, 17953 (1994).
[17] G. Kresse and J. Furthmüller, Efficient iterative schemes for ab initio total-energy calculations using a plane-wave basis set, Phys. Rev. B **54**, 11169 (1996).
[18] H. J. Monkhorst and J. D. Pack, Special points for Brillouin-zone integrations, Phys. Rev. B **13**, 5188 (1976).
[19] J. Heyd, G. E. Scuseria, and M. Ernzerhof, Hybrid functionals based on a screened Coulomb potential, J. Chem. Phys. **118**, 8207 (2003).
[20] K. Parlinski, Z. Li, and Y. Kawazoe, First-Principles Determination of the Soft Mode in Cubic ZrO_2, Phys. Rev. Lett. **78**, 4063 (1997).
[21] A. Togo, F. Oba, and I. Tanaka, First-principles calculations of the ferroelastic transition between rutile-type and $CaCl_2$-type SiO_2 at high pressures, Phys. Rev. B **78**, 134106 (2008).
[22] R. D. King-Smith and D. Vanderbilt, Theory of polarization of crystalline solids, Phys. Rev. B **47**, 1651 (1993).
[23] See Supplemental Material at http://link.aps.org/supplemental/10.1103/PhysRevApplied.11.064063 for lattice dynamics of pentasilicene (Text S1); determination of the sign of spring stiffness, Coulomb repulsive force constant, and Coulomb attractive force constant (Text S2); *T* pentasilicene on metal substrate (Text S3); band structure of pentasilicene (Fig. S4); formation of dipoles in *T* pentasilicene (Text S4); antiferroelectric configuration in *T* pentasilicene (Fig. S6); and relationship between the polarization *P* and height of dimer tilting *h* in pentasilicene (Text S5).
[24] A. Scholze, W. G. Schmidt, and F. Bechstedt, Structure of the diamond (111) surface: Single-dangling-bond versus triple-dangling-bond face, Phys. Rev. B **53**, 13725 (1996).
[25] K. C. Pandey, New π-Bonded Chain Model for Si(111)-(2×1) Surface, Phys. Rev. Lett. **47**, 1913 (1981).
[26] F. Bechstedt, A. A. Stekolnikov, J. Furthmuller, and P. Kackell, Origin of the Different Reconstructions of Diamond, Si, and Ge(111) surfaces, Phys. Rev. Lett. **87**, 016103 (2001).
[27] Z. Wang, M. Zhao, X.-F. Zhou, Q. Zhu, X. Zhang, H. Dong, A. R. Oganov, S. He, and P. Grünberg, Prediction of novel stable 2D-silicon with fivefold coordination, arXiv preprint arXiv:1511.08848 (2015).
[28] P. Borlido, C. Roedl, M. A. L. Marques, and S. Botti, The ground state of two-dimensional silicon, 2D Mater. **5**, 035010 (2018).
[29] M. Naseri, J. Jalilian, and A. Reshak, Electronic and optical properties of pentagonal-B_2C monolayer: A first-principles calculation, Int. J. Mod. Phys. B **31**, 1750044 (2017).
[30] S. Zhang, J. Zhou, Q. Wang, and P. Jena, Beyond graphitic carbon nitride: Nitrogen-rich penta-CN_2 sheet, J. Phys. Chem. C **120**, 3993 (2016).
[31] H. Liu, G. Qin, Y. Lin, and M. Hu, Disparate strain dependent thermal conductivity of two-dimensional penta-structures, Nano Lett. **16**, 3831 (2016).
[32] P. A. Fleury, J. F. Scott, and J. M. Worlock, Soft Phonon Modes and the 110° K Phase Transition in $SrTiO_3$, Phys. Rev. Lett. **21**, 16 (1968).
[33] Y. Guo, Q. Wang, Y. Kawazoe, and P. Jena, A new silicon phase with direct band gap and novel optoelectronic properties, Sci. Rep. **5**, 14342 (2015).
[34] R. Resta, Macroscopic polarization in crystalline dielectrics: The geometric phase approach, Rev. Mod. Phys. **66**, 899 (1994).
[35] C. Xiao, F. Wang, S. A. Yang, Y. Lu, Y. Feng, and S. Zhang, Elemental ferroelectricity and antiferroelectricity in group-V monolayer, Adv. Funct. Mater. **28**, 1707383 (2018).
[36] R. Fei, W. Kang, and L. Yang, Ferroelectricity and Phase Transitions in Monolayer Group-IV Monochalcogenides, Phys. Rev. Lett. **117**, 097601 (2016).
[37] J. C. Wojdel and J. Iniguez, Testing simple predictors for the temperature of a structural phase transition, Phys. Rev. B **90**, 014105 (2014).
[38] R. A. Wolkow, Direct Observation of an Increase in Buckled Dimers on Si(001) at Low Temperature, Phys. Rev. Lett. **68**, 2636 (1992).
[39] J. Dabrowski and M. Scheffler, Self-consistent study of the electronic and structural properties of the clean Si(001) (2×1) surface, Appl. Surf. Sci. **56–8**, 15 (1992).
[40] Y. Fukaya and Y. Shigeta, Phase Transition From Asymmetric to Symmetric Dimer Structure on the Ge(001) Surface at High Temperature, Phys. Rev. Lett. **91**, 126103 (2003).
[41] L. Gavioli, M. G. Betti, and C. Mariani, Dynamics-Induced Surface Metallization of Si(100), Phys. Rev. Lett. **77**, 3869 (1996).
[42] M. Poulsen and S. Ducharme, Why ferroelectric polyvinylidene fluoride is special, IEEE Trans. Dielectr. Electr. Insul. **17**, 1028 (2010).
[43] Y. J. Park, S. J. Kang, B. Lotz, M. Brinkmann, A. Thierry, K. J. Kim, and C. Park, Ordered ferroelectric PVDF-TrFE thin films by high throughput epitaxy for nonvolatile polymer memory, Macromolecules **41**, 8648 (2008).